Materials Today Bio 24 (2024) 100928

Contents lists available at ScienceDirect

Materials Today Bio

journal homepage: www.journals.elsevier.com/materials-today-bio

Dual aldehyde cross-linked hyaluronic acid hydrogels loaded with PRP and NGF biofunctionalized PEEK interfaces to enhance osteogenesis and vascularization

Junyan An [a,d,1], Xiaotong Shi [b,c,1], Jun Zhang [a], Le Qi [e], Wu Xue [a], Xinyu Nie [a], Zhihe Yun [a], Peibiao Zhang [b,**], Qinyi Liu [a,*]

[a] The Second Hospital of Jilin University, Department of Orthopedics, Changchun, 130041, China
[b] Key Laboratory of Polymer Ecomaterials, Changchun Institute of Applied Chemistry, Chinese Academy of Sciences, Changchun, 130022, China
[c] The First Hospital of Jilin University, Department of Orthopedics, Changchun, 130021, China
[d] The Third Hospital of Jilin University, Department of Neurosurgery, Changchun, 130031, China
[e] The Yunlong Orthopedic Hospital of Baotou, Department of Orthopedics, Baotou, 014010, China

ARTICLE INFO

Keywords:
Polyetheretherketone
Platelet-rich plasma
Nerve growth factor
Osteointegration
Vascularization

ABSTRACT

Polyetheretherketone (PEEK) material has become a potential bone replacement material due to its elastic modulus, which is close to that of human bone, and stable chemical properties. However, its biological inertness has hindered its clinical application. To improve the biological inertia of PEEK material, a hyaluronic acid (HA) hydrogel coating loaded with platelet-rich plasma (PRP) and nerve growth factor (NGF) was constructed on the surface of PEEK material in this study. After the hybrid hydrogel coating was constructed, scanning electron microscopy (SEM), energy dispersive spectroscopy (EDS), Fourier transform infrared spectroscopy (FT-IR), degradation tests, and enzyme-linked immunosorbent assays (ELISAs) were used to evaluate its characteristics and biological properties. The osteogenic and angiogenic potentials were also investigated in vitro and in vivo. Our results showed that the HA hydrogel loaded with RPP and NGF on the PEEK surface degraded slowly and could sustainably release various growth factors, including NGF. The results of in vitro tests showed that the hybrid hydrogel on the surface of PEEK effectively promoted osteogenesis and angiogenesis. The in vivo experiment also confirmed that the PEEK surface hydrogel could promote osseointegration of the implant and the integration of new bone and neovascularization. Our results suggest that the cross-linked hyaluronic acid hydrogel loaded with PRP and NGF can significantly improve the biological inertia of PEEK material, endowing PEEK material with good osteogenic and angiogenic ability.

1. Introduction

Due to the limitations of traditional metallic and ceramic implants, polymers have been considered candidates for implants [1–3]. Polyetheretherketone (PEEK), a semicrystalline synthetic polymer consisting of aromatic rings connected by ether and ketone groups [4], has attracted much attention in the biomedical field because of its excellent mechanical properties and resistance to degradation [5]. In particular, the elastic modulus of PEEK (~3 GPa) is comparable to that of human bone (3–17 GPa) [6], which avoids the problem of "stress shielding" and reduces the incidence of implant-induced osteoporosis [7]. In addition, PEEK is radiolucent, providing an advantage for detecting the healing process in the tissue surrounding the implant [8,]. More importantly, PEEK is the optimal thermoplastic material for orthopedic applications owing to its thermal/chemical stability and nontoxicity [9,10].

However, the inherent bioinert nature and highly hydrophobic nature of PEEK limits its performance in terms of cellular affinity and osseointegration [11,12]. Therefore, surface modification of PEEK has become one of the challenges for clinical applications [13]. This is a way to enhance bioactivity without impacting its overall structure and properties [14,15].

Platelet-rich plasma (PRP) is an autologous platelet concentrate that

* Corresponding author. Department of Orthopedic Surgery, The Second Hospital of Jilin University, 130041, Changchun, Jilin, China.
** Corresponding author.
E-mail addresses: zhangpb@ciac.ac.cn (P. Zhang), qinyi@jlu.edu.cn (Q. Liu).
[1] These authors have contributed equally to this work and share first authorship.

https://doi.org/10.1016/j.mtbio.2023.100928
Received 23 October 2023; Received in revised form 18 December 2023; Accepted 20 December 2023
Available online 25 December 2023

can be easily harvested from autologous blood and avoids autoimmune and interindividual transmission of infectious diseases [16]. α plasmids in PRP secrete a variety of growth factors, including platelet-derived growth factor (PDGF), transforming growth factor-β (TGF-β), insulin-like growth factor (IGF-1), and vascular endothelial growth factor (VEGF), among others [17,18]. They synergistically promote the regeneration and repair of cells and stroma in damaged tissues [19] and promote vascular regeneration [20] and bone tissue restoration and regeneration [21]. PRP is a safe and effective treatment modality; therefore, the sustained release of PRP on the PEEK surface to promote bone restoration is a feasible approach to improve the bioinert nature of PEEK.

Neurotrophins (NTs) include nerve growth factor (NGF), brain-derived neurotrophic factor (BDNF), neurotrophin-3 (NT-3) and NT-4 [22]. NGF is a peptide growth factor for the proliferation and differentiation of neuronal and nonneuronal cells [23]. Currently, NGF has been proven to have an important role in bone healing [24,25]. NGF and its receptors are widely expressed in skeletal tissues, which include growth plates, articular cartilage and bone [26,27]. Many studies have also identified the expression of NGF and its receptors at the site of fracture injury [27]. Previous studies have shown that NT-3, as an NT, can promote vascularization by enhancing the expression of vascular endothelial growth factor [28], and NGF has also been shown to have the ability of angiogenesis promotion [29]. Therefore, it is of great interest to investigate the sustained release of NGF from the surface of PEEK to promote bone formation and whether it can promote vascularization.

However, 95 % of the PRP and NGF started to decrease at 60 min [30] and were gradually released completely after 24 h [31]. Therefore, it is important to achieve a sustained release of PRP and NGF from PEEK surface-modified implants to achieve long-term promotion of bone regeneration and vascularization.

Hyaluronic acid (HA) is a type of polysaccharide and is an important natural polymer [32]. However, the absence of cell-binding structural domains in HA results in poor cell adhesion [33]. Previous studies have shown [34] that dialdehyde hyaluronic acid not only has good biocompatibility and biodegradability but also promotes cell adhesion and is widely used for drug delivery as a carrier substance with excellent performance for the sustained release of PRP and NGF [35].

In this study, we constructed three-dimensional (3D) porous PEEK functionalized interfaces by dialdehyde hyaluronic acid loaded with PRP and NGF (SP-DH-PRP-NGF) to promote bone regeneration and vascularization. After gaseous sulfur trioxide-induced controlled sulfonation [36], a microtopography was formed on the PEEK surface, which not only facilitated the loading and delivery of PRP and NGF but also improved osseointegration [37,38]. In vitro MC3T3 and human umbilical vein endothelial cell (HUVEC)/material coculture models were used to evaluate the effects of SP-DH-PRP-NGF on cell adhesion, viability, proliferation, osteogenic differentiation, and vascularization. An in vivo rat tibial bone defect model was used to assess the direct osteogenic and angiogenic properties.

2. Materials and methods

2.1. Synthesis and characterization of samples

2.1.1. Preparation of surface microtopography PEEK films

According to the previous research results of our group, gaseous sulfur trioxide (SO_3) was used to induce sulfonation [36]. Briefly, PEEK (15*15*0.2 mm^3) was placed in glassware, and 200 mg of P_2O_5 was added to the bottom. Then, 15 ml of H_2SO_4 was titrated into the glassware through a constant voltage funnel to produce SO_3. The whole process was carried out in an oil bath at 130 °C and protected by nitrogen under vacuum. The reaction was terminated after 15 min and washed with deionized water, ethanol, and acetone and dried at room temperature. The reaction was washed with deionized water, ethanol, acetone, ultrasonication for 10 min and dried at room temperature (SP).

2.1.2. Amino functionalization of SP

The amino functionalization of peek was synthesized and modified according to published methods [39]. Briefly, 120 ml of EDA was added to a round bottom flask equipped with a reflux condenser and heated to 125 °C. SP was then immersed in EDA at 125 °C for 4 h, removed from the reaction solution, and washed with deionized water, isopropanol, and deionized water for 10 min each. Finally, it was dried naturally at room temperature (SP–NH_2).

2.1.3. Preparation of PRP

Blood samples were collected from SD rats weighing 240 g–300 g. All experimental procedures were approved by the Animal Research Committee. The extraction of autologous PRP was performed using a two-step centrifugation technique. Ten milliliters of rat apical blood was mixed with 2 ml of citrulline. Whole blood was removed to determine platelet counts. Samples were then centrifuged at 2000×*g* for 3 min at 21 °C, and the plasma was transferred to sterile tubes and centrifuged a second time at 5000×*g* for 5 min at 21 °C. Approximately 1 ml of plasma was allowed to mix with the precipitated platelets to form PRP, and the platelet counts were measured as 5 times that of whole blood platelets.

2.1.4. Preparation of SP-H-PRP-NGF

First, oxidized HA was prepared according to a previous method [40]. Briefly, HA at a concentration of 1 % (w/v) was dissolved in double-distilled water and stirred until complete dissolution, and then 2.67 % sodium periodate (NaIO4) was added to react in a dark environment for at least 4 h. Finally, 0.5 ml of ethylene glycol was used to terminate the reaction. The oxidized HA was next purified by a dialysis procedure. Double-distilled water was used as dialysis buffer and replaced thrice per day for three days. The final oxidized HA product was obtained through freeze-drying. The degree of oxidation of HA was approximately 64 %.

Then, a 6 % solution of oxidized HA and an 8 % solution of ADH were added to a 24-well plate containing SP-NH2. After shaking for 40 min at room temperature (100 rpm), the substrate was washed three times with phosphate buffered saline (PBS) to obtain SP-HA. Twenty-five microliters of PRP was dripped during the shaking process to synthesize SP-HA-PRP samples. To prepare SP-H-PRP-NGF samples, an oxidized HA solution was prepared with PBS containing 0.5 % NGF. and 25 μl of PRP was added during shaking. To determine the optimal concentration of NGF in the mixed hydrogel, we simultaneously constructed samples with different NGF concentrations (0.1 %, 0.3 %, 0.5 %, 1 %, 3 %, 5 %).

2.1.5. Morphology observations and elemental distribution of samples

The surface micromorphology of PEEK substrates was examined by scanning electron microscopy (SEM, XL30 FEG, Philips). All PEEK substrates were sputter-coated with gold in advance. Energy dispersive X-ray spectrometry (EDX, XL-30 W/TMP, Philips, Japan) was used to further determine the elemental composition of PEEK substrates.

2.1.6. Fourier transform infrared spectroscopy

Fourier transform infrared (FTIR, Bio-Rad Win-IR spectrometer, UK) spectrometry was used to detect chemical groups. The FTIR spectra were obtained in the wavelength range of 400–4000 cm^{-1} with a resolution of 4 cm^{-1}.

2.1.7. Hydrophilicity of the sample

The hydrophilicity of the PEEK substrates was determined from measurements of the contact angle system (Kruss, DSA100, Germany). 20 μl of pure water was used for each measurement and at least five separate points on each substrate were selected for measurement, finally the outcomes were expressed as the mean and standard deviation.

2.1.8. Swelling and degradability evaluation

To assess the swelling rate of the hydrogel on the material surface, the samples were freeze-dried and weighed (W_1) and then immersed in PBS at 37 °C. Samples were removed at a preset time, and excess PBS was absorbed with filter paper and weighed (W2). The swelling rate was calculated as follows: Swelling ratio (%) = (W_2–W_1)/W_1 × 100 %.

The degradation properties of the materials were evaluated by degradation experiments. Briefly, samples were immersed in PBS at 37°, weighed after complete swelling (W_1), removed at a predetermined time and weighed after removal of excess water (W_t). The degradation rate equation is as follows: Degradation ratio (%) =(W_1-W_t)/W_1 × 100 %.

2.1.9. Thickness and adhesion of mixed hydrogels

The thickness of the mixed gel was measured using a vernier caliper. The thickness difference of PEEK sample before and after hydrogel construction is the hydrogel thickness.

The hydrogel adhesion was tested according to previous studies [41]. In brief, the adhesion performance was tested via a PosiTest AT-M adhesion tester (DeFelsko Corporation, American). First, a steel metal dolly was vertically attached to the PEEK sample (15*15*0.2 mm) with epoxy glue. A cutting tool is then used to cut the cryogel around the test dolly up to a substrate. Finally, the adhesion tester is placed on the dolly for adhesion test and record.

2.1.10. VEGF and NGF release in vitro

VEGF is one of the major growth factors released by PRP and is often used to evaluate the growth factor release capacity of PRP [42]. Therefore, the amount of VEGF and NGF released from the samples was determined by enzyme-linked immunosorbent assay (ELISA), and the absorbance was measured at 450 nm. To be briefly, PEEK disks with mixed hydrogel were placed into 24-well plates, and after 1 ml sterile PBS solution was added to each well, the plates were incubated at 37 °C. The PBS solution was collected and stored at 20 °C at preset time points (0, 2, 4, 8, 12, 24 h) and an equal volume of new PBS solution was added to the wells. Finally, cumulative release of VEGF and NGF was calculated.

2.2. In vitro studies

2.2.1. In vitro biocompatibility studies

CCK-8 was used to determine the proliferation and viability of the cells. MC3T3-E1 cells and HUVECs (2 × 104) were cultured on the surface of PEEK samples in 24-well plates for 1, 3 and 7 days, and 1 % CCK-8 solution was added to the 24-well cell/sample coculture plates. After incubation for 2 h, 100 μl of supernatant was transferred to a 96-well plate, and the optical density (OD) values were evaluated by an enzyme-labeling instrument (BioTech) at 450 nm wavelength.

To further evaluate the cytotoxicity of the samples, MC3T3-E1 cells and HUVECs were cocultured with the material for 3 days, and cell viability was determined with calcein-AM/ethidium (calcein AM/PI) and observed under a fluorescence microscope. ImageJ (NIH, Bethesda, MD) was used to perform quantitative analysis.

2.2.2. Cytoskeletal staining

The morphology of the cells on the surface of the material was observed by DAPI and rhodamine B-phalloidin. MC3T3-E1 cells and HUVECs were inoculated into 24-well plates at a density of 2 × 10^4. After coculture with the samples for 1 day, the cells were fixed with 4 % paraformaldehyde for 30 min, washed 3 times with PBS to remove residual paraformaldehyde and permeabilized with 0.5 % Triton X-100 for 10 min. The actin filaments were stained with rhodamine B-phalloidin (Cytoskeleton, Inc., USA), and the nuclei were stained with DAPI (Solarbio, China). Observation of the cytoskeleton by fluorescence microscopy.

2.2.3. Alkaline phosphatase (ALP) staining and quantification

An ALP color development kit (Beyotime) and ALP assay kit (Beyotime) were used to stain and quantify the ALP activity. MC3T3-E1 was inoculated at 2*10^4 on the surface of PEEK samples in 24-well plates and incubated for 7 and 14 days. Subsequently, the cells were fixed with 4 % paraformaldehyde for 30 min and incubated with preconfigured BCIP/NBT dye for 1 h. The dye was removed by washing 3 times with PBS. The image was captured through a light microscope.

For ALP quantification , After the cells are cultured for a predetermined time, place the well plate on an ice box, remove the medium, rinse three times with PBS and add 200 μl of cell lysate (without inhibitor), freeze–thaw twice, add 50 μl of lysate and 50 μl of pNPP reagent in a 96-well plate, incubate for 30 min and measure the absorbance value at 405 nm (OD405).

The total protein contained in the lysate was also measured by a BCA kit. The BCA solution was mixed at A:B = 50:1, and 200 μl of BCA solution and 20 μl of cell lysate were added to a 96-well plate and incubated for 30 min. The OD value was measured at 562 nm (OD562), and the final expression of ALP in each group was expressed as OD405/OD562.

2.2.4. Alizarin red S (ARS) staining and quantification

ARS was used to measure the ability of mineralized nodule formation. Briefly, MC3T3-E1 cells were cocultured with samples for 14 and 21 days and then fixed in 95 % ethanol for 1 h. A 2 % ARS (pH = 4.2) solution was then added to 24-well plates and incubated for 30 min, and unreacted ARS was rinsed thoroughly with distilled water. The images were captured by light microscopy. The stained samples were then dripped into a 1 % (w/v) hexadecylpyridinium chloride reaction for 1 h. One hundred microliters of the suspension was transferred to a 96-well plate, and the OD value was measured at 570 nm.

2.2.5. Tubule formation assay

Fifty microliters of Matrigel matrix (BD, United States) was mixed with DMEM at a 1:1 ratio, added to a 24-well plate and incubated at 37° for 30 min to form a gel state. HUVECs were resuspended using cell/material extracts, inoculated on the Matrigel surface and incubated for 24 h. Pictures were taken under an inverted microscope (Olympus Corporation, Japan), and the results were quantified using ImageJ.

2.2.6. Cell invasion assay

After 24 h of serum-free incubation with HUVECs, 100 μl of cell suspension (2 × 10^4) was added to the upper chamber. Samples and 500 μl of complete medium were added to the lower chamber. After incubation for 24 h, the cells were fixed with 4 % paraformaldehyde for 30 min and washed 3 times with PBS. Residual cells in the upper chamber were wiped with a cotton swab. The cells were stained with 1 % crystal violet for 10 min and then observed under an inverted microscope. The results were analyzed using ImageJ software.

2.2.7. Wound healing assay

HUVECs were inoculated in 6-well plates (10 × 10^6) and incubated for 24 h. Scratches of the same width were introduced in the 6-well plates with a 200 μl pipette and washed three times with PBS. The 6-well plate was then incubated at 37 °C and 5 % CO2 for 24 h, the wound healing variability was assessed under a microscope, and quantitative analysis was performed with ImageJ software.

2.2.8. RT–qPCR

To further verify the osteogenic and angiogenic properties of the material, the expression levels of typical osteogenic genes (RUNX2, Col-I and OPN) in each group of samples were examined by quantitative real-time polymerase chain reaction (QRT-qPCR) on day 14. The expression of the angiogenic genes Bax, Bcl-2 and MMP-2 was assayed on day 4. Relative mRNA expression was measured using the $2^{-\Delta\Delta Ct}$ method and was normalized to endogenous GAPDH levels.

2.3. In vivo studies

Animal experiments were approved by the animal ethics committee. Twenty male SD rats were required for this study and were randomly divided into 5 groups (n = 4): PEEK, SP, SP-H, SP-H-PRPRP, and SP-H-PRP-NGF. Rats were anesthetized with 10 % chloral hydrate. After shaving, the skin was incised, and a defect 2.5 mm in diameter and 3 mm in depth was created in the tibial plateau area using a bone drill. Different samples were implanted into the bone defect. Finally, the skin was sutured, and antibiotics were injected for 3 consecutive days. The procedure was strictly aseptic.

2.3.1. Micro-CT analysis

The rats were sacrificed at 4 and 8 weeks postoperatively, and the tibiae were obtained. The tibia was scanned and reconstructed by micro-CT. Images were viewed by 3D visualization software (Skyscan 1076 Scanner, Bruker Micro-CT, NV, Kontich, Belgium), and BV/TV was statistically analyzed by CTAn software (SkyScan, Belgium).

2.4. Histological analysis

After specimens were obtained, they were fixed in 4 % paraformaldehyde for 48 h and decalcified for 45 days. Bone tissue was embedded in paraffin and sectioned. Then, new bone, blood vessels and collagen were evaluated by hematoxylin & eosin (HE) staining. Immunofluorescence staining was used to analyze the expression of genes associated with osteogenesis and angiogenesis. Images of the sections were captured by an imaging system (NIKON DS-U3, Japan).

2.5. Statistical analysis

At least three samples were included in each group, and the results are expressed as the mean plus standard deviation. Differences between multiple experimental groups were examined by one-way analysis of variance (ANOVA) and Tukey's multiple comparison test. GraphPad Prism (v8.0.2) was used for all statistical analyses. $P < 0.05$ indicated statistical significance.

3. Results

3.1. Characterization of the HA/PRP/NGF coating on the SP surface

The number of platelets in whole blood was $6.54 \pm 0.21 \times 10^{11}$, and that in PRP was $35.15 \pm 0.18 \times 10^{11}$. The concentration of platelets in PRP was 5.37 times that in whole blood. The SEM results showed the surface morphology of different groups of samples (Fig. 1A-1E). The surface of the PEEK group was smooth and flat. Surface micropores were observed in the SP group. After freeze-drying, cross-linked hyaluronic acid showed a loose and large pore structure on the surface of the PEEK material. After adding PRP, the pore structure on the surface of the SP-H-PRP group samples was small and dense. The pore structure of the sample surface in the SP-H-PRP-NGF group was consistent with that in the SP-H-PRP group, indicating that the addition of NGF did not change the structure of the mixed coating of HA and PRP. The EDS results show the elemental distribution on the surface of each sample (Fig. 1. F-Fig. 1J). It can be seen that only the sample of the SP group contained 6.28 wt% S on the surface. On the surface of the SP-H group, S disappeared, and N appeared at 8.95 wt%. With the addition of PRP, the surface N content of the SP-H-PRP group further increased to 10.17 wt%. Finally, the addition of NGF again increased the surface N content to 11.17 wt%.

The water contact angle is one of the important means to evaluate the surface hydrophilicity of materials (Fig. 2A). The results of this study show that the water contact angle on the surface of the material in the PEEK group is $86.40 \pm 1.18^{\circ}$, which is significantly higher than that in the other four groups. The surface water contact angle of PEEK treated

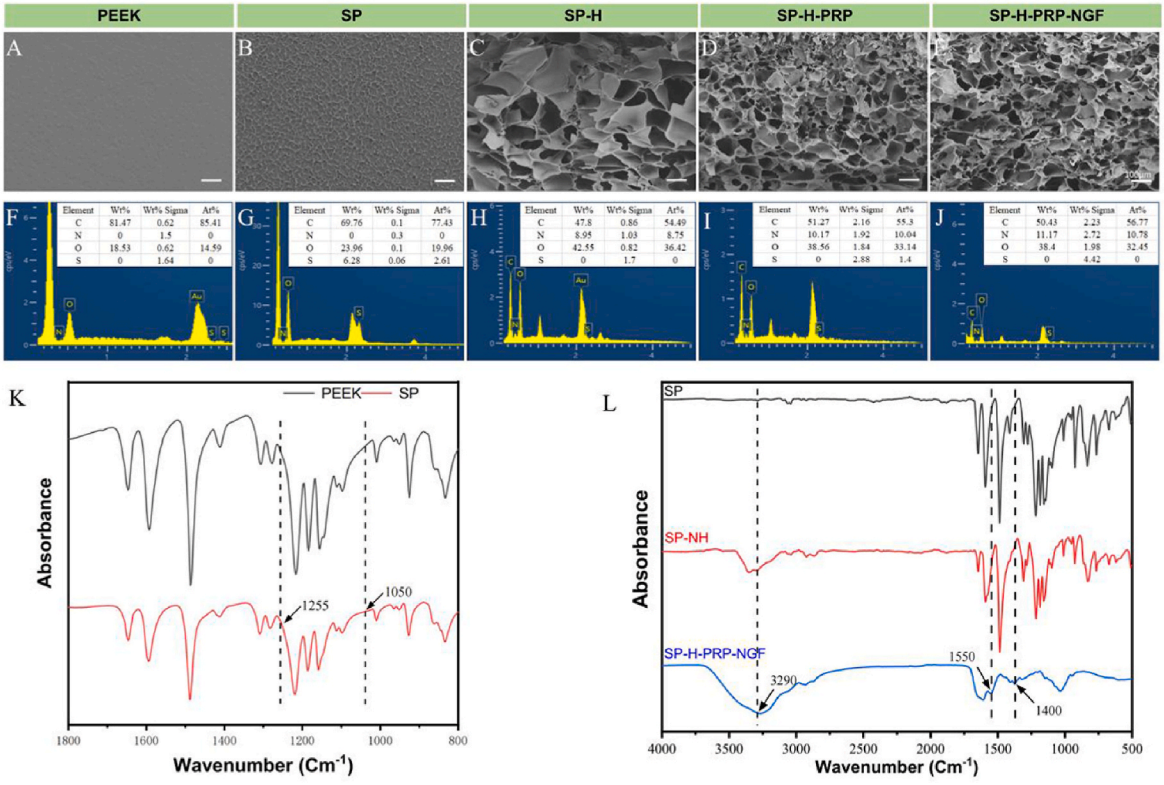

Fig. 1. (A–E) The SEM morphology of different PEEK interfaces from left to right. (F–J) Results of EDS elemental content analysis of different PEEK interfaces. (K–L) FT-IR results of different PEEK interfaces.

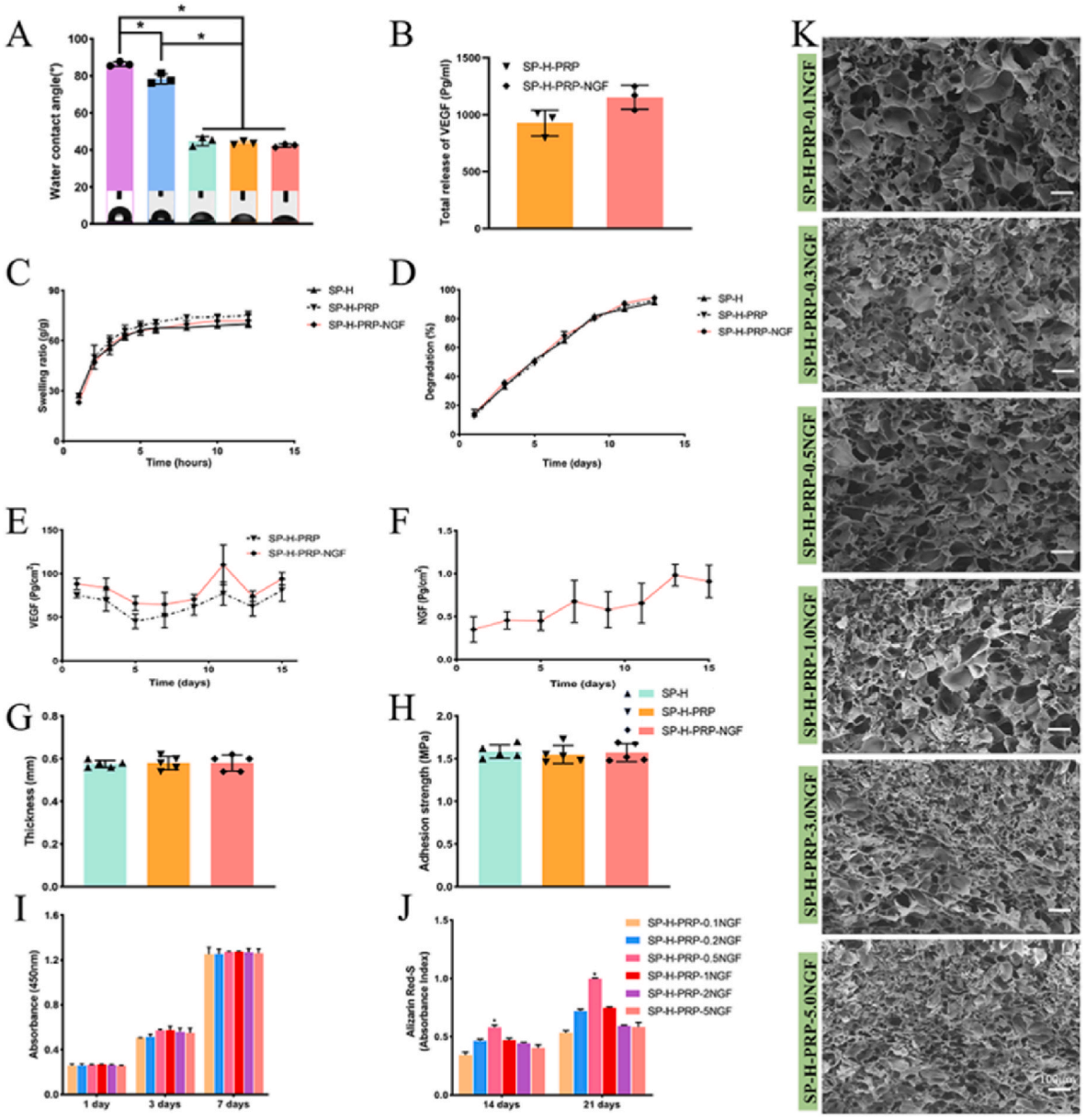

Fig. 2. (A) Water contact angle of different PEEK interfaces, n = 5. (B) VEGF total release amount of SP-H-PRP group and SP-H-PRP-NGF group. (C) Hydrogel swelling ratio of SP-H, SP-H-PRP and SP-H-PRP-NGF groups, n = 3. (D) The degradation curve of SP-H, SP-H-PRP and SP-H-PRP-NGF groups, n = 3. (E) Cumulative VEGF release curve of SP-H-PRP group and SP-H-PRP-NGF group, n = 3. (F) Cumulative NGF release curve of SP-H-PRP-NGF group, n = 3.(G) The hydrogel thickness of SP-H,SP-H-PRP and SP-H-NGF groups, n = 5. (H)The hydrogel adhesion strength of SP-H,SP-H-PRP and SP-H-NGF groups,n = 5.(I) CCK-8 results of MC3T3-E1 cells at day 1, 3, and 7, n = 3. (J) 14 days and 21 days of ARS quantitative analysis results, n = 3. (K) SEM images of mixed gels on PEEK surface with different NGF content.* indicates $p < 0.05$.

with sulfur trioxide was 78.33 ± 2.75°, which was significantly higher than that of the SP-H, SP-H-PRP and SP-H-PRP-NGF groups. The water contact angles of the SP-H, SP-H-PRP and SP-H-PRP-NGF groups were 44.67 ± 2.41°, 43.60 ± 0.92° and 42.30 ± 0.92°, respectively, and there was no significant difference among them. The hydrogel thickness of SP-H,SP-H-PRP and SP-H-NGF groups was 0.58 ± 0.02, 0.58 ± 0.03 and 0.58 ± 0.04 mm respectively, and no statistical difference was found (Fig. 2G). The hydrogel adhesion of SP-H,SP-H-PRP and SP-H-NGF groups was 1.58 ± 0.08,1.55 ± 0.11 and 1.57 ± 0.10 MPa respectively, and no statistical difference was found (Fig. 2H).

The results of Fourier transform infrared (FT-IR) spectroscopy show the chemical characteristics of the surface of the samples in each group. In Fig. 1K and Fig. 1. L, the characteristic peaks of all PEEK materials are shown, including the diketobenzene band at positions 1650 cm-1, 1490 cm-1 and 926 cm-1; the C–O–C stretching vibration of diaryl groups at positions 1188 cm-1 and 1158 cm-1; and the C═C of the benzene ring in PEEK at 1600 cm-1. In addition to the above characteristic peaks, the sample of the SP group showed an O═S═O-related peak at 1255 cm-1 and an S═O-related peak at 1050 cm-1 (Fig. 1K) [33]. Both SP-NH and SP-H-PRP-NGF samples showed the characteristic peak of –NH at 3290 cm-1 [37]. Compared with the SP-N group, the SP-H-PRP-NGF group showed the characteristic N–H bending peak and C–H bending peak after HA cross-linking at 1550 and 1400, respectively (Fig. 1L) [43].

In this study, we tested the swelling rate of hydrogels with different compositions on the PEEK surface. The results showed that the swelling rate of the hydrogel on the surface of the samples in each group was stabilized after the freeze-dried samples were immersed in PBS solution for 12 h. At 12 h, the swelling rates of samples from the SP-H, SP-H-PRP

and SP-H-PRP-NGF groups were 69.98 ± 2.04 %, 74.97 ± 2.70 % and 72.08 ± 3.37 %, respectively (Fig. 2C). The swelling rate curve trend of the hydrogel in each group was basically the same, which showed that water absorption was fast before 6 h, and water absorption was slow and tended to be stable after 6 h. We also investigated the degradation rate of each group of hydrogels on the PEEK surface. The degradation rate curves of the hydrogel on the surface of the three groups were consistent and close to linear degradation. On the 13th day, the degradation rates of hydrogel on the surface of all the samples reached more than 90 %, which were 91.44 ± 0.26 %, 92.72 ± 0.64 % and 94.55 ± 0.48 %, respectively (Fig. 2D).

The release of VEGF in the SP-H-PRP group and SP-H-PRP-NGF group was evaluated by ELISA. NGF release from the SP-H-PRP-NGF group was also assessed at the same time points. The results showed that the release of NGF in the SP-H-PRP-NGF group was relatively consistent at different time points, and the overall trend was irregular waves (Fig. 2F). The release of VEGF in the SP-H-PRP group and SP-H-PRP-NGF group at different time points was also relatively consistent, and the trend of the release curve of VEGF in the two groups was basically the same (Fig. 2E). The amount of VEGF released was higher in the SP-H-PRP-NGF group than in the SP-H-PRP group at each time point, and although the total amount of VEGF released was higher in the SP-H-PRP-NGF group than in the SP-H-PRP group, there was no significant difference between the two groups (Fig. 2B).

In order to explore the optimal dose of NGF to exert biological activity in the mixed gel on PEEK surface. We set up groups with different NGF content, and observed the morphology and structure of different groups of PEEK surface mixed gels under SEM. The results showed that when the NGF content reached 3 % and 5 %, the pore structure of hydrogel becomes small and dense. (Fig. 2K). At the same time, we used CCK-8 and ARS quantitative assay to evaluate the effects of different levels of NGF on the proliferation and differentiation of MC3T3-E1 cells (Fig. 2I). The results showed that the increasing NGF content in the mixed gel on PEEK surface did not show a trend of increasing the proliferation of MC3T3-E1 cells. The ARS quantitative results showed that when the NGF content of PEEK surface mixed gel was 0.5 %, the mixed gel had the strongest ability to promote cell differentiation (Fig. 2J). Therefore, in the following experiment, we chose 0.5 % NGF concentration.

3.2. In vitro cell experiments

3.2.1. Biocompatibility of SP-HA/PRP/NGF with MC3T3-E1 and HEUVC cells

Live and dead staining was used to evaluate the compatibility of samples from each group with MC3T3-E1 cells and HEUVC cells (Fig. 3B). Our results showed that the number of adherent cells on the surface of the samples in the PEEK and SP groups was low. The cell adhesion ability of the hyaluronic acid group was slightly improved, and the number of cells was increased compared with the previous two groups. The number of adherent cells on the surface of the SP-H-PRP group and SP-H-PRP-NGF group was significantly higher than that of the other three groups. Our quantitative analysis results showed that the addition of HA, PRP and NGF significantly increased the cell count ratio on the sample surface (Fig. 3. E and Fig. 3F). This is consistent with our observations above. It was concluded that the addition of hyaluronic acid, PRP and NGF could improve the cytocompatibility.

To further evaluate the cell adhesion ability of the materials, the nucleus and cytoskeleton of the two cell lines were stained with DAPI and Action-Tracker Red, respectively (Fig. 3A). Most of the cells on the surface of the samples in the PEEK and SP groups were oval, and no pseudopodia were observed. Consistent with the previous results, with the addition of HA, PRP and NGF, the number of nuclei on the surface of the sample increased. Moreover, with the addition of HA, PRP and NGF,

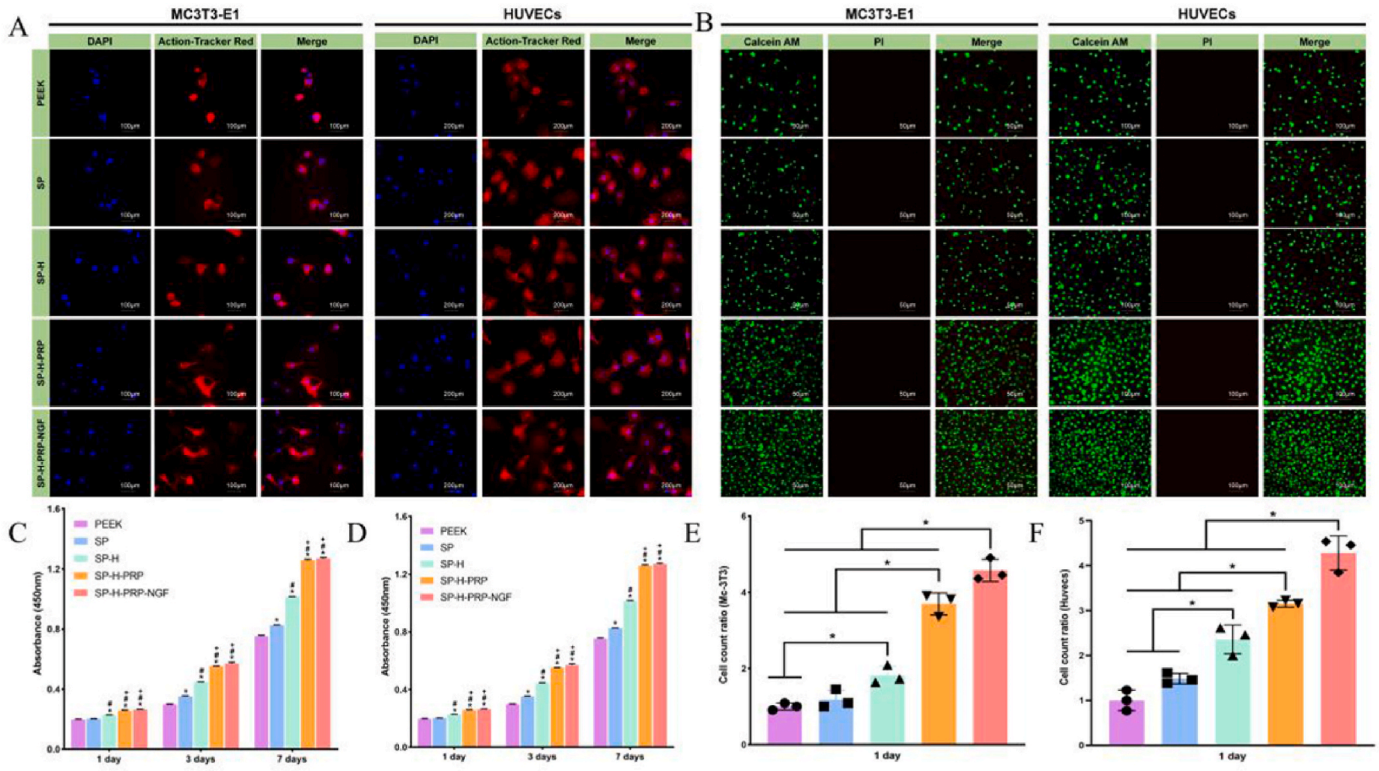

Fig. 3. (A) Action-Tracker Red and DAPI staining results of MC3T3-E1 and HUVEC from different groups. (B) Live and dead staining results of MC3T3-E1 and HUVEC from different groups. (C) CCK-8 results of MC3T3-E1 at day 7 and day 14, n = 3. (D) CCK-8 results of HUVEC at day 7 and day 14, n = 3. (E–F) Cell count ratio of MC3T3-E1 and HUVEC at 1 day, n = 3. *, #, + and ++ indicates value of the group is significant higher than that of PEEK group, SP group, SP-H group, SP-H-PRP group respectively, $p < 0.05$. (For interpretation of the references to color in this figure legend, the reader is referred to the Web version of this article.)

cytoskeletal spreading became increasingly extensive. Especially after the addition of PRP and NGF, the cells extended filopodia. These results indicated that HA, PRP and NGF could improve the adhesion of MC3T3-E1 cells and HUVECs to PEEK materials.

A CCK-8 assay was used to evaluate the ability of each material surface pair to promote the proliferation of both cell types (Fig. 3. C and Fig. 3D). Compared with the PEEK group, the SP group did not show a significant increase in cell proliferation on the first day. On the 3rd and 7th days, the proliferation of the SP group was significantly higher than that of the PEEK group. The samples in the SP-H group showed significantly enhanced cell proliferation ability compared with the other two groups at 1, 3, and 7 days, indicating that the hyaluronic acid gel on the surface of the material promoted cell proliferation. Compared with the former three groups, the SP-H-PRP group also showed a significantly enhanced ability to promote the proliferation of both cell lines at 1, 3 and 7 days. It was proven that the addition of PRP further enhanced the pro-proliferation ability of PEEK materials. However, compared with the SP-H-PRP group, the SP-H-PRP-NGF group did not show further enhanced proliferation ability of either cell line. These results indicated that NGF could not enhance the proliferation of MC3T3-E1 and HEUVC cells.

3.2.2. *The HA/PRP/NGF gel on the PEEK surface promoted osteogenesis*

Alkaline phosphatase (ALP) activity is one of the indicators used to evaluate osteoblast differentiation. In this study, MC3T3-E1 cells were cultured on the surface of each sample for 7 days and 14 days for ALP staining and quantitative analysis. In the ALP staining results, the blue part represents ALP, and the bare white is the original surface of the samples in each group (Fig. 4A). The blue area on the surface of each group expanded and deepened in color with the extension of time. At the same time, with the sulfonation of the PEEK surface and the addition of HA, PRP and NGF, the surface staining area of the samples in the SP, SP-H, SP-H-PRP and SP-H-PRP-NGF groups gradually increased, and the staining color gradually deepened. These results suggested that gaseous sulfur trioxide sulfonation, HA, PRP and NGF could promote osteogenic differentiation. This was also confirmed by quantitative analysis of ALP (Fig. 4B).

Extracellular matrix mineralization is one of the key markers of late osteogenic differentiation of cells. In this study, the osteogenic differentiation ability of the samples was further evaluated by staining and quantitative analysis of the surface cells with alizarin red-S dye. As shown, calcium nodules in the cellular matrix were stained orange−red (Fig. 4C). At each time point, with the addition of PEEK sulfonation, HA, PRP and NGF, the orange-stained calcium nodules on the surface of the materials increased, and staining also became darker. The results of quantitative ARS analysis were consistent with those of staining.

To further evaluate the ability of samples from each group to contribute to osteogenic differentiation, we examined the expression levels of osteogenic genes on the surface of samples from each group by RT−qPCR. The expression levels of three osteogenic genes, Runx2, Col1 and OPN, were consistent in the surface cells of each group (Fig. 4D–F). The results showed that the expression level of SP group was not significantly higher than that in the PEEK group. However, the expression level of osteogenic genes in the SP-H group was significantly higher than that in the PEEK and SP groups, indicating that HA promoted the expression of osteogenic genes in MC3T3-E1 cells. The expression levels

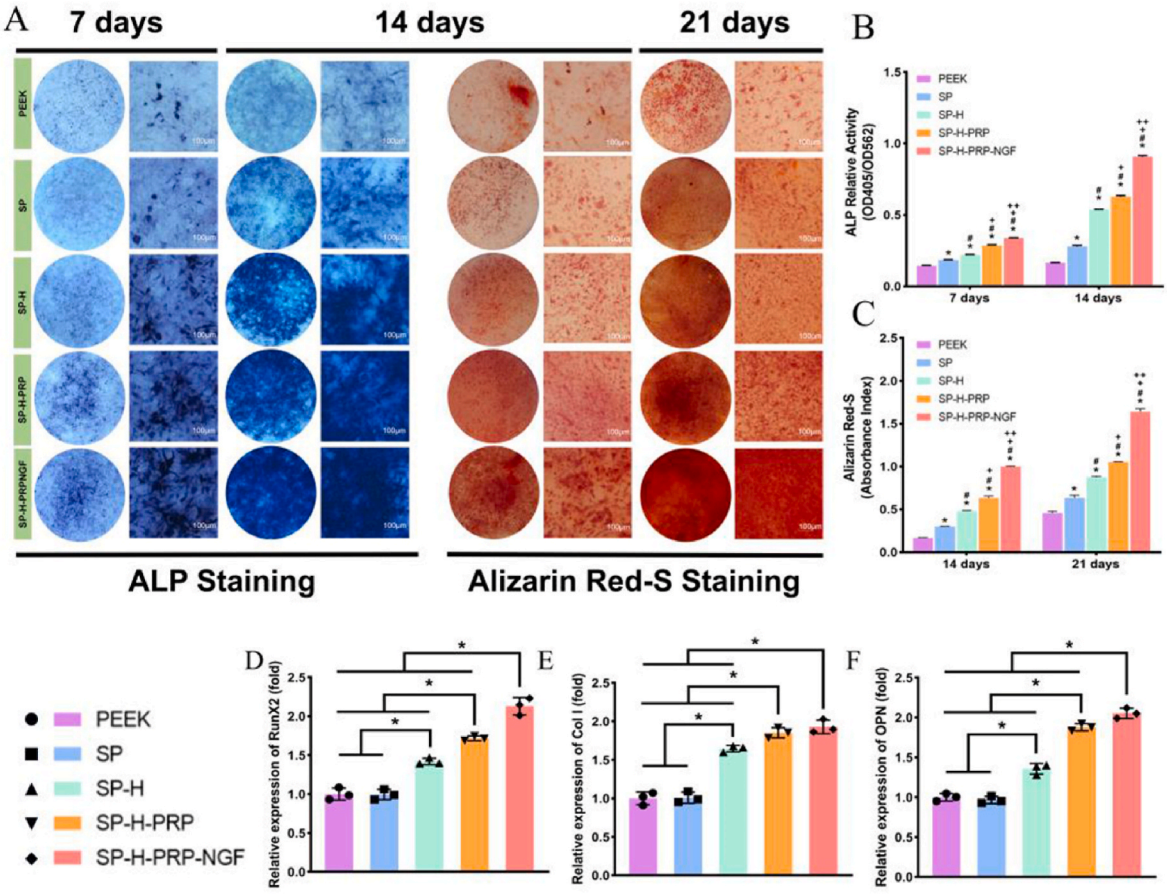

Fig. 4. (A) Alkaline phosphatase (ALP) staining and alizarin red-S (ARS) staining results at 7 days and 14 days of each group. (B) Quantitative analysis of ALP of each group, n = 3. (C) Quantitative analysis of ARS of each group. (D–F) RT-qPCR analysis of Runx2, Col1 and OPN genes*, #, + and ++ indicates value of the group is significant higher than that of PEEK group, SP group, SP-H group, SP-H-PRP group respectively, n = 3, $p < 0.05$. (For interpretation of the references to color in this figure legend, the reader is referred to the Web version of this article.)

of osteogenic genes in the surface cells of the SP-H-PRP group samples were significantly higher than those in the previous three groups, indicating that PRP also has the ability to promote osteogenic differentiation of MC3T3-E1 cells. Similarly, the expression levels of the three osteogenic genes in the surface cells of the samples in the SP-H-PRP-NGF group were significantly higher than those in the other four groups, indicating that NGF also has the ability to promote osteogenic differentiation.

3.2.3. HA/PRP/NGF gel on PEEK surface promoted angiogenesis

Wound healing assays were used to evaluate the migration ability of HUVECs on the surface of each sample (Fig. 5. A and Fig. 5D). The results showed that the SP group did not enhance the cell migration ability compared with the PEEK group. However, the cell migration ability of the SP-H group was significantly stronger than that of the PEEK and SP groups. The cell migration ability of the SP-H-PRP group was significantly higher than that of the other three groups. The cell migration ability of the SP-H-PRP-NGF group samples was significantly higher than that of the other four groups. These results indicated that HA, PRP and NGF could promote HUVEC migration.

The cell invasion assay further evaluated the migratory ability of HUVECs on the surface of each sample. As shown in Fig. 5. C, with the addition of HA, PRP and NGF, an increasing number of cells penetrated the polycarbonate membrane. The results of quantitative analysis showed that the cell penetration rates of the PEEK, SP, SP-H, SP-H-PRP and SP-H-PRP-NGF groups were 1 ± 0.02, 1.31 ± 0.07, 2.03 ± 0.31, 3.53 ± 0.20 and 4.65 ± 0.61, respectively (Fig. 5H). The cell penetration rate of the SP-H-PRP-NGF group was significantly higher than that of the other four groups. The cell penetration rate of the SP-H-PRP group was significantly higher than that of the PEEK, SP, and SP-H groups. The cell penetration rate of the SP-H group was significantly higher than that of the PEEK and SP groups. This indicated that the addition of HA, PRP and NGF enhanced the chemotaxis of PEEK materials.

The ability of samples from each group to promote HUVECs to form tubules was assessed by tube formation assay. As shown in Fig. 5. B, Fewer intact tubules were formed in the PEEK, SP and SP-H groups.

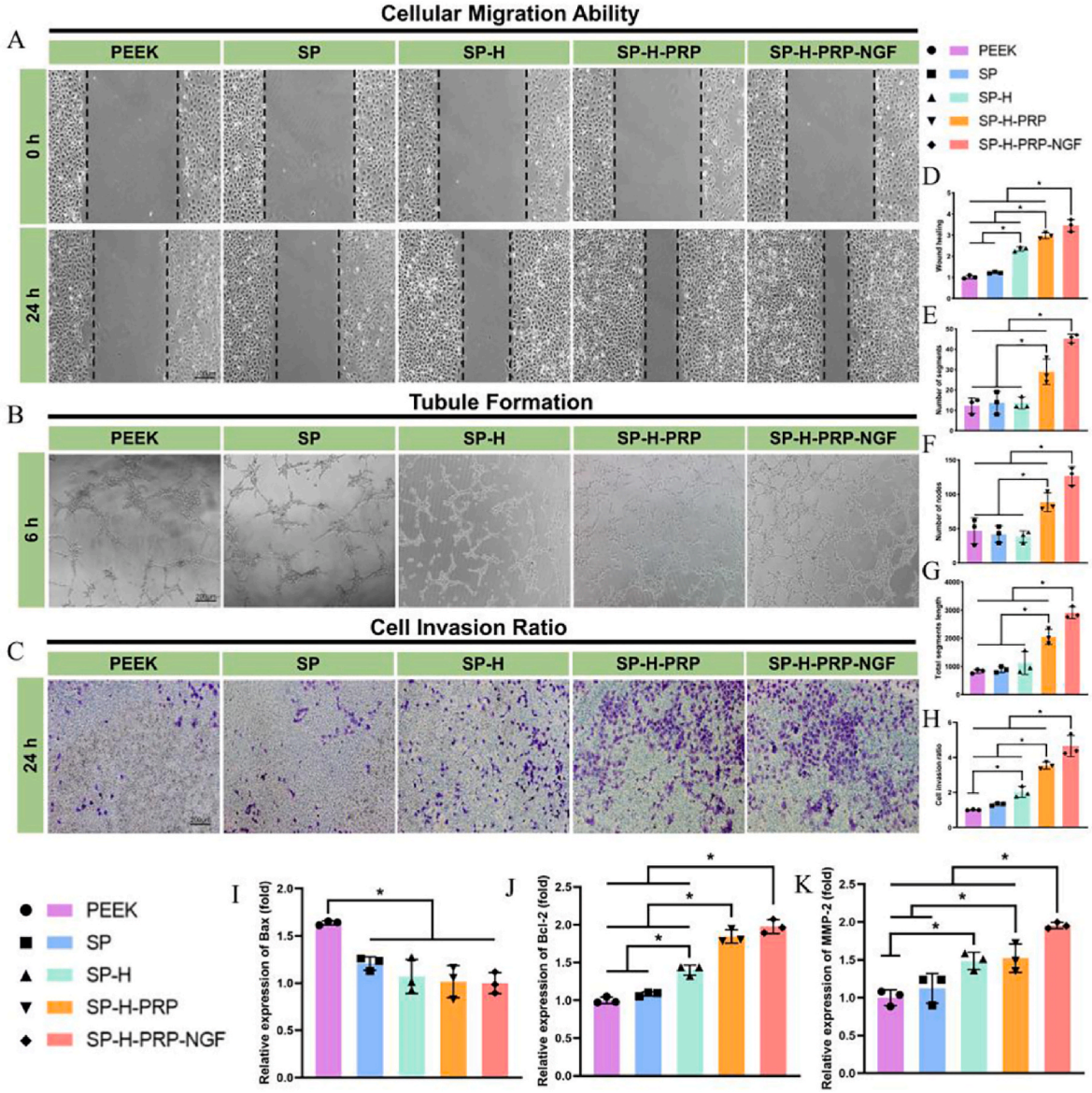

Fig. 5. (A) Wound healing assay results of each group with HUVEC cells. (B) Tube formation results of each group with HUVEC cells. (C) Cell invasion assay results of each group with HUVEC cells. (D) Quantitative analysis of wound healing assay from each group, n = 3. (E–G) Quantitative analysis of the number of nodes, the number of segments and the total length of segments from each group, n = 3. (H) Cell invasion ratio results of each group, n = 3. (I–K) RT-qPCR analysis of Bax, Bcl-2 and MMP-2 genes, n = 3.* indicates $p < 0.05$.

However, dense and intact tubules were observed in the SP-H-PRP and SP-H-PRP-NGF groups. The number of nodes, the number of segments and the total length of segments were quantitatively analyzed (Fig. 5E–G). The results showed that there was no significant difference among the PEEK group, SP group and SP-H group. The number of nodes, the number of segments and the total length of segments in the SP-H-PRP group were significantly higher than those in the other three groups. The number of nodes, the number of segments and the total length of segments in the SP-H-PRP-NGF group were significantly higher than those in the other four groups. These results indicate that the ability of PEEK, sulfonated PEEK surface and hyaluronic acid to induce HUVECs to form tubules is limited. PRP and NGF have a good ability to promote HUVECs to form tubules.

To further assess the effect of samples from each group on angiogenesis, RT−qPCR analysis was performed on HUVECs cultured on the surface of samples from each group (Fig. 5I-K). MMP-2 is an angiogenic gene, and Bcl-2 and Bax are apoptosis-related genes, among which Bcl-2 inhibits apoptosis and Bax promotes apoptosis. The results showed that the expression level of Bax in the PEEK group was significantly higher than that in the other four groups. The expression level of Bcl-2 in the SP-H-PRP-NGF group was significantly higher than that in the PEEK, SP and SP-H groups, but no significant difference was found between the SP-H-PRP group and SP-H-PRP-NGF group. The expression level of MMP-2 in the SP-H-PRP-NGF group was significantly higher than that in the other four groups. These results prove that dual aldehyde cross-linked hyaluronic acid hydrogels loaded with PRP and NGF biofunctionalized PEEK interfaces enhanced vascularization in vitro.

3.3. In vivo animal testing

3.3.1. Microcomputed tomography (Micro-CT) evaluation

After surgery, bone formation in the tibia of rats implanted with PEEK was evaluated by X-ray at 4 and 8 weeks after surgery (Fig. 6A). The results show that PEEK material exhibits good radiotransparent, and the arrow in the figure shows the location of PEEK material. Cortical bone shadow around PEEK material showed new bone formation around PEEK material in all groups at 4 and 8 weeks after surgery. In the present study, cylindrical samples of each group were implanted in the tibial defect model of SD rats. The tibial specimens were collected at 4 and 8 weeks, fixed with paraformaldehyde, and scanned by micro-CT. Three-dimensional reconstruction of the data obtained after scanning was performed, and quantitative analysis of various osteogenic indexes was performed to evaluate the osteogenic ability of each group in vivo. The 3D images of the PEEK implant and its surrounding new bone after 3D reconstruction are shown in Fig. 6B; the gray−white cylinders are PEEK samples from each group, and the blue part is the surrounding new bone. We can see that for the samples of the same group, the amount of new bone at 8 weeks was significantly greater than that at 4 weeks, and the new bone coverage area on the surface of the samples at 8 weeks was larger. At 4 weeks, there was no significant increase in new bone mass in the SP group compared with the PEEK group. However, with the addition of HA, PRP and NGF, the amount of new bone in the SP-H, SP-H-PRP and SP-H-PRP-NGF groups increased. At 8 weeks, the amount of new bone in the SP group was significantly greater than that in the PEEK group. The amount of new bone in the SP-H, SP-H-PRP and SP-H-PRP-NGF groups increased. All of them were significantly higher than those in the former two groups. Then, the trabecular bone volume

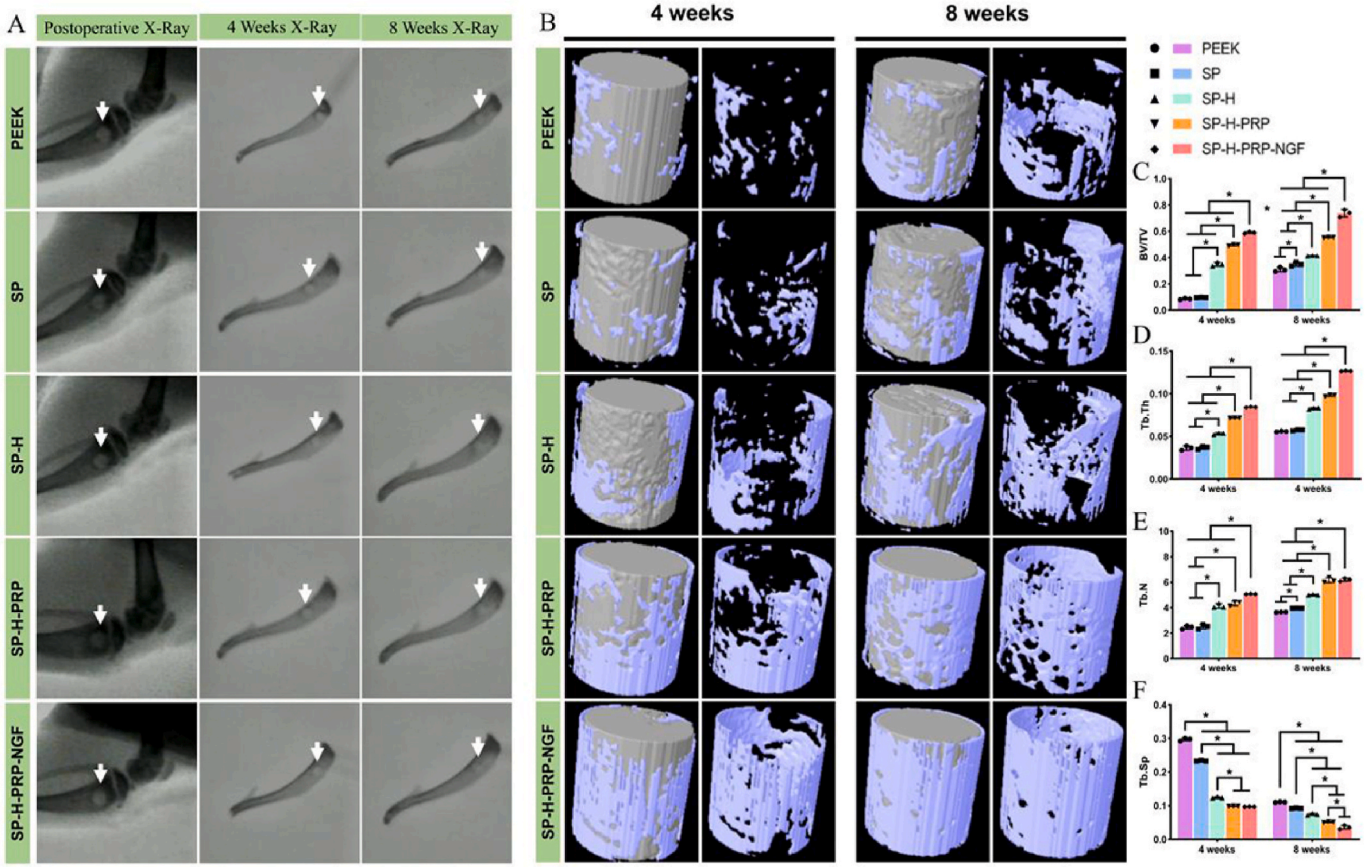

Fig. 6. (A)X-ray images of tibia of rats in each group after PEEK implantation at postoperative, 4 weeks and 8 weeks, the arrow indicates the location of the PEEK implant.(B)3D reconstruction of new bone of each group at 4 weeks and 8 weeks. (C–F) Quantitative analysis of trabecular bone volume fraction (BV/TV), trabecular bone number (Tb·N), trabecular bone thickness (Tb·Th) and trabecular bone separation (Tb.Sp), n = 3. * indicates $p < 0.05$.

fraction (BV/TV), trabecular bone number (Tb·N), trabecular bone thickness (Tb·Th) and trabecular bone separation (Tb.Sp) were used to quantify the new bone formation of each group (Fig. 6C-F). At 4 weeks, there was no significant difference in the above four indexes between the SP group and the PEEK group. BV/TV, Tb·Th, and Tb·N of the SP-H, SP-H-PRP and SP-H-PRP-NGF groups gradually increased significantly. The trend of Th. Sp in each group was opposite to that described above. At 8 weeks, BV/TV, Tb·Th, and Tb·N in the SP group were significantly higher than those in the PEEK group, and Tb. Sp was significantly lower than that in the PEEK group. At 8 weeks, the trends of the four indexes in the SP-H, SP-H-PRP and SP-H-PRP-NGF groups were the same as those at 4 weeks. These results indicate that gaseous sulfur trioxide on the surface of PEEK, HA, PRP and NGF has a certain osteogenic effect in vivo. Moreover, dual aldehyde cross-linked hyaluronic acid hydrogels loaded with PRP and NGF biofunctionalized PEEK interfaces could enhance osteogenesis in vivo.

3.3.2. *HE staining results*

The tibial samples of each group at 8 weeks were fixed and decalcified, and the PEEK implants were removed for sectioning and HE staining. The staining results are shown in Fig. 7A. P represents the location of the PEEK implant, NB represents the new bone as a ring surrounding the implant, BV represents the blood vessel, and BM represents the location of the medullary cavity. It could be observed that the new bone in the PEEK group was less, did not form a complete ring, and the new bone ring formed was thin, and no angiogenesis was observed in the new bone. In the SP group, a complete ring was basically formed, but the new bone ring was still thin, and a small number of new bone vessels could be seen. Both the SP-H and SP-H-PRP groups formed complete new bone rings with moderate thickness, and the bone rings in the SP-H-PRP group were thicker than those in the SP-H group. Blood vessels were observed in the new bone ring in both groups. The bone ring in the SP-H-PRP-NGF group was significantly thicker than that in the other groups, and large blood vessels were observed in the bone ring. The above results show that dual aldehyde cross-linked hyaluronic acid hydrogels loaded with PRP and NGF biofunctionalized PEEK interfaces could enhance osteogenesis and vascularization in vivo.

3.3.3. *Results of immunofluorescence staining*

To further evaluate the in vivo osteogenic potential of the samples, tibial specimens collected at week 8 were sectioned and stained for OCN and OPN immunofluorescence. Fig. 7B shows the results of OCN immunofluorescence staining, with nuclei in blue–purple and OCN expression levels in red. The expression level of OCN in the PEEK group was the lowest. In the SP group, OCN showed intermittent expression and did not form a ring around the implant. The expression of OCN in the SP-H group basically formed a complete ring. In the SP-H-PRP group, the OCN expression lines formed complete rings, and the thickness of the expression rings increased significantly. The SP-H-PRP-NGF group had the thickest ring of OCN expression. Fig. 7C shows the expression results of OPN in samples of each group, and the expression trend of each group was consistent with that of OCN in each group. The relative staining intensity results for OCN and OPN are shown in Fig. 8. C and Fig. 8D. In conclusion, HA hydrogels loaded with RPR and NGF on PEEK surfaces significantly promoted the expression of OCN and OPN in vivo.

To further evaluate the angiogenic ability in vivo, tibial specimens collected at week 8 were sectioned and stained with CD31 and CD34 immunofluorescence. CD34 staining results showed that the expression of CD34 around the implants in the PEEK group was the lowest (Fig. 8A). The expression of CD34 in the SP, SP-H and SP-H-PRP groups increased gradually but did not form a complete expression ring. CD34 expression in the SP-H-PRP-NGF group was the highest and formed a complete expression ring. CD31 staining showed that the expression of CD31 in the PEEK, SP, SP-H, SP-H-PRP and SP-H-PRP-NGF groups increased gradually, even though CD31 expression rings were formed in all groups (Fig. 8B). The relative staining intensity results for OCN and OPN are shown in Fig. 8. E and Fig. 8F. These results indicate that HA hydrogels loaded with PRP and NGF on the surface of PEEK could promote angiogenesis.

4. Discussion

When the human body has bone defects, especially massive bone defects and tooth loss, the choice of bone replacement materials is very important for the repair of bone defects. At present, the commonly used

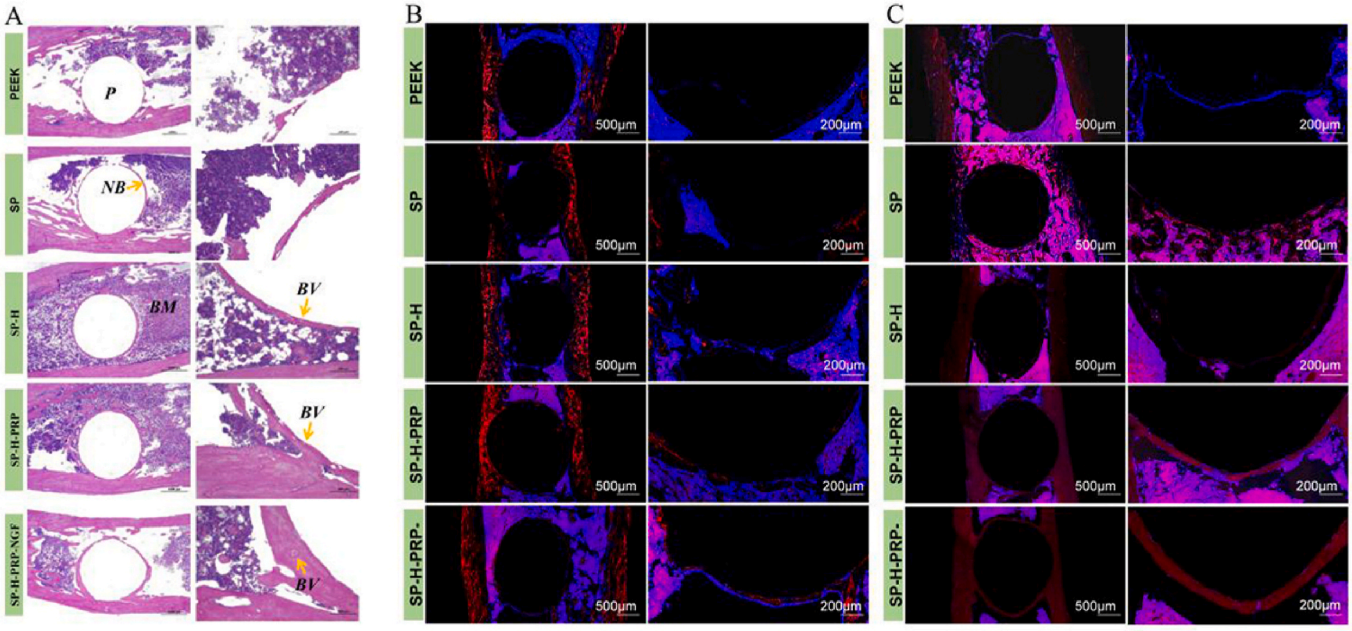

Fig. 7. (A) HE staining results of tibial samples from each group at 8 weeks. P represents the location of the PEEK implant, NB represents the new bone as a ring surrounding the implant, BV represents the blood vessel, and BM represents the location of the medullary cavity. (B–C) Results of OPN, OCN immunofluorescence staining of each group at 8 weeks. The red part represents OPN and OCN staining, and the blue-purple part is nuclear staining. (For interpretation of the references to color in this figure legend, the reader is referred to the Web version of this article.)

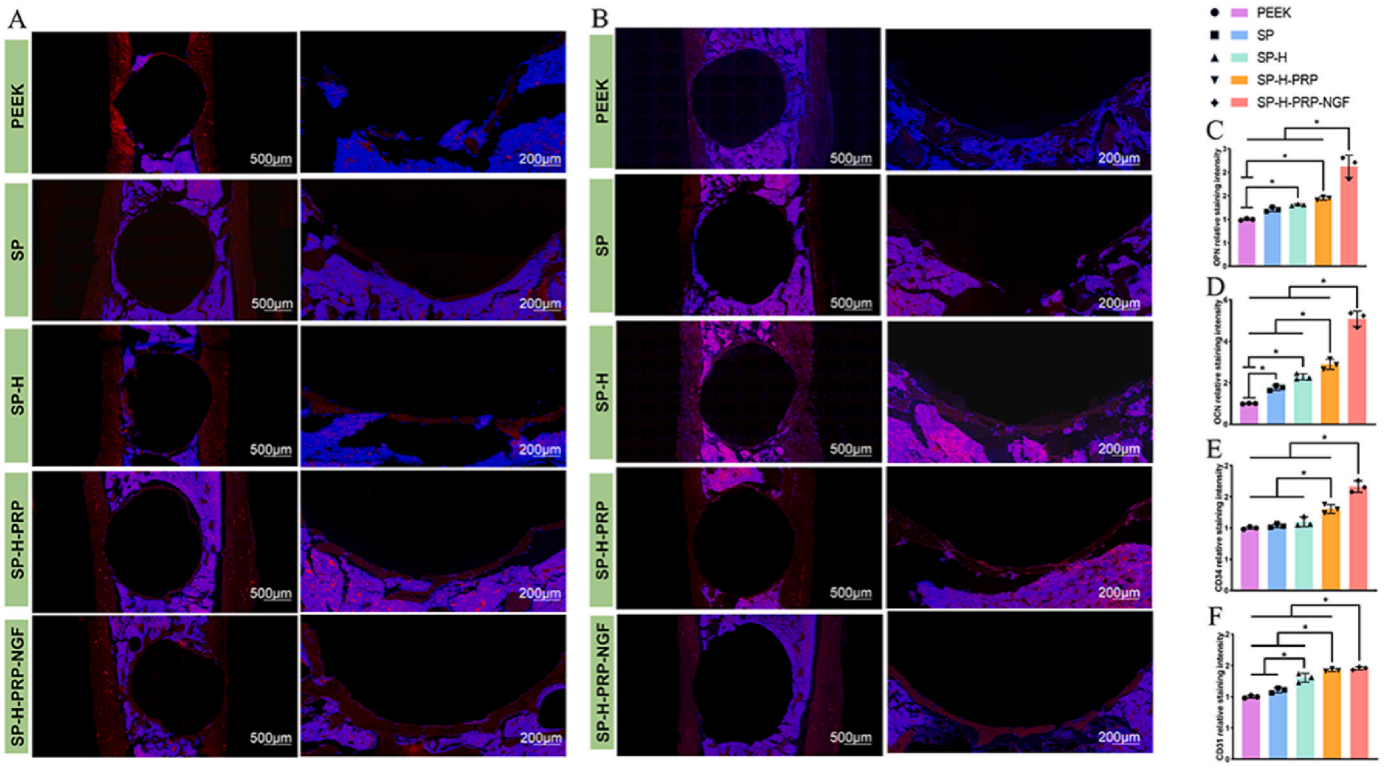

Fig. 8. (A) Results of CD31 immunofluorescence staining of each group at 8 weeks. The red part represents CD31 staining, and the blue-purple part is nuclear staining. (B) Results of CD34 immunofluorescence staining of each group at 8 weeks. The red part represents CD34 staining, and the blue-purple part is nuclear staining. (C–F) The relative staining intensity results for OPN, OCN, CD31 and CD34 of each group at 8 weeks, n = 3. * indicates $p < 0.05$. (For interpretation of the references to color in this figure legend, the reader is referred to the Web version of this article.)

bone replacement materials include titanium, ceramics, and allogeneic bone. However, their high elastic modulus, high fragility, and high cost limit their application and development. Studies have shown that PEEK material has the characteristics of a low elastic modulus, radiation permeability and chemical stability and is a potential bone replacement material. However, the inherent biological inertness of PEEK itself hinders its clinical application [44]. Therefore, it is necessary to modify the bioactivity of PEEK materials. In this study, NGF-reinforced PRP was loaded on PEEK, and its osteogenic and angiogenic potentials were evaluated in vitro and in vivo. At the same time, considering that osseointegration of the material surface is a long-term process, we used dialdehyde cross-linked hyaluronic acid as the carrier of NGF and PRP to achieve a sustained release effect.

First, we modified the morphology of the PEEK surface with gaseous sulfur trioxide. SEM images showed that the honeycomb structure appeared on the surface of the modified PEEK, and EDS results showed that the S element increased on the surface of the SP group. The addition of the -SO3 group was confirmed by the O═S═O peak at 1255 cm^{-1} and the S═O peak at 1050 cm^{-1} in the subsequent FT-IR results. However, -SO3 is a hydrophilic group, so the water contact angle of the SP group is significantly lower than that of the PEEK group. This is consistent with the results of our previous study [36]. The honeycomb structure brought by gaseous sulfur trioxide on the surface of PEEK is not only conducive to the bonding of the PEEK surface and hydrogel but also enhances the bonding force between PEEK and bone after the hydrogel is dissolved in vivo. At the same time, the reduced hydrophobicity of the PEEK surface is conducive to the adhesion and growth of osteocytes. Next, to combine hyaluronic acid with PEEK more closely and make the hyaluronic acid spread more evenly on the PEEK surface, ethylene diamine was used to reduce the amino groups on the PEEK surface [39]. The amino groups on the PEEK surface can undergo a Schiff base reaction with the aldehyde groups in HA. The success of the reaction was demonstrated by the –NH peak at 3290 in the FR-IR results. We then prepared dialdehyde-crosslinked hyaluronic acid on the amino-functionalized PEEK surface. SEM results showed that the samples in the SP-H group had loose and irregular pore structures after freeze-drying, which was conducive to cell adhesion and growth [45]. The water contact angle results showed that the hydrophilicity of PEEK was significantly enhanced by the addition of hyaluronic acid. The degradation test showed that the degradation rate of the HA hydrogel on the surface of the SP-H group was 91.44 ± 0.26 % at 13 days, indicating that the HA hydrogel had the ability to degrade slowly. The release curves of VEGF and NGF demonstrated the sustained release ability of the HA hydrogel mixed with the PEEK surface. The same levels of VEGF and NGF released at different time points confirmed the linear degradation of the hybrid hydrogel. The same trend of VEGF release in the SP-H-PRP group and SP-H-PRP-NGF group indicated that the addition of NGF did not change the degradation characteristics of the mixed gel. Although there was no significant difference in total VEGF release between the two groups, the total VEGF release was higher in the SP-H-PRP-NGF group than in the SP-H-PRP group. This may be because the released NGF has a certain activating effect on the released platelets and the chimeric platelets on the hydrogel surface, and the better activated platelets release more growth factors [46].

PRP is an autologous-derived blood extract, and the main component is enriched platelets. Therefore, compared with other animal-derived bioactive factors, it is more biosafe. When activated in vivo, PRP can release a large number of growth factors, including platelet-derived growth factor, transforming growth factor and vascular endothelial growth factor [17,18]. PRP has been clinically used in several fields, and there are considerable studies using it in combination with hydrogels [45,47,48]. However, the application of PRP on the surface of PEEK materials has rarely been studied. In theory, PRP itself has the ability to promote bone formation, angiogenesis and immune regulation, which

almost perfectly solves the problem of biological activity modification and immune rejection of bone substitute material implants. In this study, PRP was used as one of the main bioactive components to improve the osteogenesis and angiogenesis of PEEK materials. In the SEM results, the diameter of the irregular pore structure formed on the surface of the samples in the SP-H-PRP group after freeze-drying was significantly smaller than that in the SP-H group. The reason for this phenomenon is not clear. Perhaps the internal cross-linking structure of HA was changed by the addition of PRP. It has been pointed out that the pore structure of hydrogels is related to ice core formation during lyophilization [49,50]. Therefore, it is also possible that the addition of PRP affected ice core formation during the freeze-drying of the mixture, ultimately resulting in inconsistent pore sizes. Because PRP is also a hydrophilic substance, the water contact angle of the SP-H-PRP group remained the same as that of the SP-H group. It is worth mentioning that the degradation curve of the HA hydrogel on the PEEK surface was consistent with that of the HA-PRP mixture. We hypothesized that this was because PRP was uniformly distributed in the system during HA shaking crosslinking after being added to the 24-well plate. In other words, PRP was not activated during HA cross-linking, and no cascade reaction was produced to cause cross-linking of collagen in PRP. Therefore, the addition of PRP did not change the degradation curve of the whole system.

Studies have shown that nerve growth factor can not only promote the proliferation and differentiation of nerve cells but also promote osteogenesis and angiogenesis by upregulating the expression of VEGF. It is well known that bone defect repair is regulated by a variety of growth factors, and osteogenesis and angiogenesis are important links in the process of implant-host integration [24,25,28]. Therefore, in this study, HA was used to carry PRP and NGF on the surface of PEEK at the same time to further increase the osteogenic and angiogenic functions of PEEK. Our results showed that the addition of NGF did not change the water contact angle or degradation curve of the HA-PRP mixture on the original PEEK surface. It is worth mentioning that when the concentration of NGF is 1 % or less, the pore structure of the mixed hydrogel is similar to that of the SP-H-PRP group. When the concentration of NGF is 3 % and 5 %, the pores of the mixed gel become small and dense. The reason why the pore structure of mixed gels changes with NGF content is not clear. Furthermore, our results showed that with the increase of the amount of NGF added, the promoting effect on the osteogenic differentiation of MC3T3 increased first and then decreased. We believe this is because osteogenic differentiation is dose-dependent before the concentration of NGF reaches 0.5 %. However, high NGF showed inhibitory effect on osteoblastic differentiation. Previous studies have shown that excess NGF secretion can be found in the joint fluid of patients with osteoarthritis [51].

In this study, the osteogenic and angiogenic abilities of each group of materials were evaluated in vitro. Our previous studies have shown that gaseous sulfur trioxide modification can increase the hydrophilicity of the PEEK surface and endow PEEK materials with a surface microstructure. The increased hydrophilicity and surface microstructure increased the cell adhesion, cell proliferation and cell differentiation ability of PEEK. In this study, the samples in the SP group had a stronger ability to promote the adhesion and proliferation of MC3T3-E1 cells and HUVECs than the samples in the PEEK group. Compared with the PEEK group, the SP-H-PRP group had a stronger ability to promote osteogenic differentiation of MC3T3-E1 cells and angiogenesis of HUVECs. Hyaluronic acid is a biodegradable macromolecular acidic mucopolysaccharide. It is a component of the extracellular matrix of connective tissue, and it is also widely found in body fluids such as joint fluid and eye glass [52,53]. Due to its good biocompatibility, mechanical strength and slow degradation characteristics, it is widely used in many medical fields, such as tissue engineering. Previous studies have shown that HA possesses good cell adhesion, osteopromoting and angiogenic abilities [54]. In this study, the samples from the SP-H group showed a better ability to promote the proliferation of MC3T3-E1 cells and HUVECs and better promote the osteogenic differentiation of MC3T3-E1 cells and angiogenesis of HUVECs than those from the PEEK group and SP group. However, the ability of HA to promote bone formation and angiogenesis is limited. In a wide range of clinical applications and research, HA is more commonly used as a drug carrier and to regulate sustained release. PRP is widely used in orthopedics, and studies have shown that RPP could promote tendon healing, cartilage repair and bone formation. The main growth factors secreted by PRP are PDGF, TGF and VEGF [16–18]. PDGF can promote the proliferation of osteocytes and the integration of bone and blood vessels; TGF can promote the proliferation and differentiation of osteocytes; and VEGF can promote vascular cell migration and angiogenesis [55–58]. The results of Nagao et al. showed that PRP perfusion can promote the maturation of vascular endothelial cells [59]. The results of this study are consistent with the above views. Compared with the PEEK, SP, and SP-H groups, the SP-H-PRP group significantly increased the osteogenic ability of MC3T3-1 cells and the angiogenic ability of HUVECs. Yada et al. showed that the addition of NGF increased ALP activity and increased collagen synthesis in MC3T3-E1 cells [60]. Mogi's study showed that NGF prevented apoptosis in MC3T3-E1 cells [61]. The latest study by Xu et al. showed that NGF can promote bone injury repair by promoting the chemotaxis of osteoblasts to damaged tissues through the p75 signaling pathway [62]. In the present study, we found that the addition of NGF increased the adhesion ability of the mixed gel on the PEEK surface to both types of cells but did not promote the proliferation of both types of cells. Although in the quantitative analysis of the proportion of cells with live and dead staining, the SP-H-PRP-NGF group was significantly higher than that in the SP-H-PRP group, there was no significant difference in the CCK-8 cell count between the two groups. The results of the ALP activity test, ARS staining and RT−qPCR showed that NGF loaded on the PEEK surface mixed gel had a good ability to promote osteogenic differentiation. NGF has also been shown to promote VEGF expression and the ability to promote endothelial cell maturation. This was confirmed by the HUVEC-related assay in the present study. In summary, dual aldehyde cross-linked hyaluronic acid hydrogels loaded with PRP and NGF biofunctionalized PEEK interfaces have a good ability to promote bone formation and angiogenesis in vitro.

Finally, an SD rat tibial defect model was established, and the cylindrical samples of each group were implanted into the bone defect site. Tibial samples were collected at 4 and 8 weeks to evaluate the in vivo osteogenic and angiogenic ability of each group. The three-dimensional reconstruction data of micro-CT visually showed new bone formation in each group. The samples in the SP-H-PRP and SP-H-PRP-NGF groups had good osteogenic ability in vivo. There was no significant difference in CT quantitative analysis between the SP and PEEK groups at 4 weeks, while the parameters of new bone formation in the SP group were significantly better than those in the PEEK group at 8 weeks. This indicates that the hydrophilicity of PEEK endowed by gaseous sulfur trioxide and the osteopromoting effect caused by the microstructure surface are weak. The results of HE staining showed that the SP-H-PRP and SP-H-PRP-NGF groups not only showed good osteogenic ability but also had a certain number of new blood vessels in the new bone. This indicated that the HA-PRP hybrid gel and HA-PRP-NGF gel on the surface of PEEK promoted angiogenesis and the integration of blood vessels and new bone. The immunofluorescence results also confirmed that the SP-H-PRP and SP-H-PRP-NGF groups had good osteogenic and angiogenic abilities in vivo. These results all indicate that dual aldehyde cross-linked hyaluronic acid hydrogels loaded with PRP- and NGF-biofunctionalized PEEK surfaces have good osteogenesis and angiogenesis abilities in vivo.

Limitations of this study: First, we did not investigate whether the pro-differentiation effect of NGF in the gel mixture on MC3T3-E1 cells and the pro-angiogenic effect on HUVECs was dose dependent. Finding the minimum dose of NGF to exert these effects can save medical resources and reduce costs. Second, the mechanism of the synergistic osteogenesis and angiogenesis between NGF and PRP was not investigated in this study. However, there are many growth factors released by PRP, and it is difficult to study the synergistic mechanism between NGF

and PRP. Third, the adhesion strength between PEEK substrate and hydrogel coating is poor and adhesion of the HA coating could further increase the binding force of PEEK with the mixed hydrogels.

5. Conclusion

As one of the main potential bone substitutes, bioactive modification of PEEK is of great importance. In this study, we fabricated a dialdehyde cross-linked hyaluronic acid hydrogel coating loaded with RPP and NGF on the surface of PEEK. The results showed the hybrid hydrogel coating on the surface of PEEK had good hydrophilicity and the ability to continuously release growth factors. In vitro cell experiments showed that the hybrid hydrogel coating had good cell adhesion and promoted the differentiation of MC3T3-E1 cells and angiogenesis of HUVECs. However, the addition of NGF did not further improve the cell proliferation ability of the hybrid hydrogel. In the rat tibial defect model, PEEK samples coated with the hybrid hydrogel also demonstrated good osteogenic and angiogenic abilities.

CRediT authorship contribution statement

Junyan An: Conceptualization, Data curation, Formal analysis, Methodology, Software, Writing - original draft, Writing - review & editing. **Xiaotong Shi:** Conceptualization, Data curation, Methodology, Software, Writing - original draft, Writing - review & editing. **Jun Zhang:** Data curation, Software, Writing - review & editing. **Le Qi:** Data curation, Formal analysis, Software. **Wu Xue:** Methodology, Software. **Xinyu Nie:** Conceptualization, Investigation. **Zhihe Yun:** Data curation, Methodology. **Peibiao Zhang:** Conceptualization, Funding acquisition, Investigation, Methodology, Project administration. **Qinyi Liu:** Conceptualization, Data curation, Funding acquisition, Project administration, Resources, Supervision.

Declaration of competing interest

Conflicts of interest: none.

The authors declare that they have no known competing financial interests or personal relationships that could have appeared to influence the work reported in this paper.

Data availability

Data will be made available on request.

Acknowledgements

This work was financially supported by Jilin Provincial Department of Science and Technology (20210101265JC) and Jilin Provincial Department of Finance (ZXWSTZXEY041).

References

[1] Y. Yu, Y. Sun, X. Zhou, Y. Mao, Y. Liu, L. Ye, et al., Ag and peptide co-decorate polyetheretherketone to enhance antibacterial property and osteogenic differentiation, Colloids Surf. B Biointerfaces 198 (2021), 111492.
[2] Zhiyong Chen, Yu Chen, Jiandong Ding, Lin Yu, Blending strategy to modify PEEK-based orthopedic implants, Composites: Part B, Eng. 250 (1–20) (2023), 110427.
[3] Z. Chen, Y. Chen, Y. Wang, J. Deng, X. Wang, Q. Wang, Y. Liu, J. Ding, L. Yu, Polyetheretherketone implants with hierarchical porous structure for boosted osseointegration, Biomater. Res. 27 (1) (2023 Jun 27) 61, https://doi.org/10.1186/s40824-023-00407-5. PMID: 37370127; PMCID: PMC10294516.
[4] S.M. Kurtz, J.N. Devine, PEEK biomaterials in trauma, orthopedic, and spinal implants, Biomaterials 28 (32) (2007) 4845–4869.
[5] L. Lin, X.-Q. Pei, R. Bennewitz, A.K. Schlarb, Friction and wear of PEEK in continuous sliding and unidirectional scratch tests, Tribol. Int. 122 (2018) 108–113.
[6] W.T. Lee, J.Y. Koak, Y.J. Lim, S.K. Kim, H.B. Kwon, M.J. Kim, Stress shielding and fatigue limits of poly-ether-ether-ketone dental implants, J. Biomed. Mater. Res. B Appl. Biomater. 100 (4) (2012) 1044–1052.
[7] R.D. Carpenter, B.S. Klosterhoff, F.B. Torstrick, K.T. Foley, J.K. Burkus, C.S.D. Lee, et al., Effect of porous orthopaedic implant material and structure on load sharing with simulated bone ingrowth: a finite element analysis comparing titanium and PEEK, J. Mech. Behav. Biomed. Mater. 80 (2018) 68–76.
[8] P. Korn, C. Elschner, M.C. Schulz, U. Range, R. Mai, U. Scheler, MRI and dental implantology: two which do not exclude each other, Biomaterials 53 (2015) 634–645.
[9] Y. Zheng, A. Gao, J. Bai, Q. Liao, Y. Wu, W. Zhang, M. Guan, L. Tong, D. Geng, X. Zhao, P.K. Chu, H. Wang, A programmed surface on polyetheretherketone for sequentially dictating osteoimmunomodulation and bone regeneration to achieve ameliorative osseointegration under osteoporotic conditions, Bioact. Mater. 14 (2022 Feb 1) 364–376, https://doi.org/10.1016/j.bioactmat.2022.01.042. PMID: 35386814; PMCID: PMC8964985.
[10] Yanyan Zheng, Huang Zhou, Mengqi Li, Jingjing Fu, Jun Dong, Ying Liu, Liu, Lvhua. Polyetheretherketone surface engineered with a degradable hybrid coating for accelerating osteogenesis, Mater. Lett. 331 (2023), 133515.
[11] M. Chen, L. Ouyang, T. Lu, H. Wang, F. Meng, Y. Yang, et al., Enhanced bioactivity and bacteriostasis of surface fluorinated polyetheretherketone, ACS Appl. Mater. Interfaces 9 (20) (2017) 16824–16833.
[12] Y. Ji, H. Zhang, J. Ru, F. Wang, M. Xu, Q. Zhou, et al., Creating micro-submicro structure and grafting hydroxyl group on PEEK by femtosecond laser and hydroxylation to synergistically activate cellular response, Mater. Des. (2021) 199.
[13] Genwen Mao, Qianqian Sun, Jiajun Jiang, Jianzhong Sun, Tao Wu, Chi Cheng, Menghao Teng, Yuqi Zhao, Xiaoling Zhou, Hao Zhang, Weiguo Bian, Dopamine and epigallocatechin-3-gallate cross-linked coating demonstrates improved osteointegration of polyetheretherketone in rabbits, Mater. Des. 226 (2023), 111607.
[14] Xinxin Bai, Xintian Zhang, Rui Zhang, Wenhao Chen, Han Wang, Jiecheng Xiao, Quan Liu, Shaohuang Weng, Min Chen, Immobilizing enoxacin on implant by polyvinyl butyral coating to promote osseointegration in osteoporosis with infection, Mater. Des. 227 (2023), 111749.
[15] Weifang Zhang, Lvhua Liu, Huang Zhou, Chanjuan He, Xueli Yang, Jingjing Fu, Huaiyu Wang, Ying Liu, Yanyan Zheng, Surface bisphosphonation of polyetheretherketone to manipulate immune response for advanced osseointegration, Mater. Des. 232 (2023), 112151.
[16] X. Liu, Y. Yang, X. Niu, Q. Lin, B. Zhao, Y. Wang, et al., An in situ photocrosslinkable platelet rich plasma - complexed hydrogel glue with growth factor controlled release ability to promote cartilage defect repair, Acta Biomater. 62 (2017) 179–187.
[17] H.T. Liao, M.J. Tsai, M. Brahmayya, J.P. Chen, Bone regeneration using adipose-derived stem cells in injectable thermo-gelling hydrogel scaffold containing platelet-rich plasma and biphasic calcium phosphate, Int. J. Mol. Sci. 19 (9) (2018).
[18] Y. Qi, L. Niu, T. Zhao, Z. Shi, T. Di, G. Feng, et al., Combining mesenchymal stem cell sheets with platelet-rich plasma gel/calcium phosphate particles: a novel strategy to promote bone regeneration, Stem Cell Res. Ther. 6 (2015) 256.
[19] V. Cervelli, P. Gentile, B. De Angelis, C. Calabrese, A. Di Stefani, M.G. Scioli, et al., Application of enhanced stromal vascular fraction and fat grafting mixed with PRP in post-traumatic lower extremity ulcers, Stem Cell Res. 6 (2) (2011) 103–111.
[20] M. Samberg, R. Stone 2nd, S. Natesan, A. Kowalczewski, S. Becerra, N. Wrice, et al., Platelet rich plasma hydrogels promote in vitro and in vivo angiogenic potential of adipose-derived stem cells, Acta Biomater. 87 (2019) 76–87.
[21] B.H. Choi, C.J. Im, J.Y. Huh, J.J. Suh, S.H. Lee, Effect of platelet-rich plasma on bone regeneration in autogenous bone graft, Int. J. Oral Maxillofac. Surg. 33 (1) (2004) 56–59.
[22] S. Sun, N.H. Diggins, Z.J. Gunderson, J.C. Fehrenbacher, F.A. White, M.A. Kacena, No pain, no gain? The effects of pain-promoting neuropeptides and neurotrophins on fracture healing, Bone 131 (2020), 115109.
[23] S.D. Skaper, The biology of neurotrophins, signalling pathways, and functional peptide mimetics of neurotrophins and their receptors, CNS Neurol. Disord.: Drug Targets 7 (1) (2008) 46–62.
[24] C.J. Xian, X.F. Zhou, Treating skeletal pain: limitations of conventional anti-inflammatory drugs, and anti-neurotrophic factor as a possible alternative, Nat. Clin. Pract. Rheumatol. 5 (2) (2009) 92–98.
[25] Y.W. Su, R. Chung, C.S. Ruan, S.M. Chim, V. Kuek, P.P. Dwivedi, et al., Neurotrophin-3 induces BMP-2 and VEGF activities and promotes the bony repair of injured growth plate cartilage and bone in rats, J. Bone Miner. Res. 31 (6) (2016) 1258–1274.
[26] A. Gigante, C. Bevilacqua, A. Pagnotta, S. Manzotti, A. Toesca, F. Greco, Expression of NGF, Trka and p75 in human cartilage, Eur. J. Histochem. 47 (4) (2003) 339–344.
[27] K. Asaumi, T. Nakanishi, H. Asahara, H. Inoue, M. Takigawa, Expression of neurotrophins and their receptors (TRK) during fracture healing, Bone 26 (6) (2000) 625–633.
[28] Y.W. Su, X.F. Zhou, B.K. Foster, B.L. Grills, J. Xu, C.J. Xian, Roles of neurotrophins in skeletal tissue formation and healing, J. Cell. Physiol. 233 (3) (2018) 2133–2145.
[29] M. Troullinaki, V.I. Alexaki, I. Mitroulis, A. Witt, A. Klotzsche-von Ameln, K. J. Chung, T. Chavakis, M. Economopoulou, Nerve growth factor regulates endothelial cell survival and pathological retinal angiogenesis, J. Cell Mol. Med. 23 (4) (2019 Apr) 2362–2371, https://doi.org/10.1111/jcmm.14002. Epub 2019 Jan 24. PMID: 30680928; PMCID: PMC6433692.
[30] Q. Chang, J. Li, Z. Dong, L. Liu, F. Lu, Quantitative volumetric analysis of progressive hemifacial atrophy corrected using stromal vascular fraction-supplemented autologous fat grafts, Dermatol. Surg. 39 (10) (2013) 1465–1473.
[31] Z. Liu, X. Yuan, G. Fernandes, R. Dziak, C.N. Ionita, C. Li, et al., The combination of nano-calcium sulfate/platelet rich plasma gel scaffold with BMP2 gene-modified

mesenchymal stem cells promotes bone regeneration in rat critical-sized calvarial defects, Stem Cell Res. Ther. 8 (1) (2017) 122.
[32] F. Munarin, M.C. Tanzi, P. Petrini, Advances in biomedical applications of pectin gels, Int. J. Biol. Macromol. 51 (4) (2012) 681–689.
[33] Y. Hu, Y. Li, F.J. Xu, Versatile functionalization of polysaccharides via polymer grafts: from design to biomedical applications, Acc. Chem. Res. 50 (2) (2017) 281–292.
[34] S. Liu, Y. Zhu, H. Gao, P. Ge, K. Ren, J. Gao, et al., One-step fabrication of functionalized poly(etheretherketone) surfaces with enhanced biocompatibility and osteogenic activity, Mater. Sci. Eng. C Mater. Biol. Appl. 88 (2018) 70–78.
[35] S. Wei, P. Xu, Z. Yao, X. Cui, X. Lei, L. Li, et al., A composite hydrogel with co-delivery of antimicrobial peptides and platelet-rich plasma to enhance healing of infected wounds in diabetes, Acta Biomater. 124 (2021) 205–218.
[36] T. Wan, Z. Jiao, M. Guo, Z. Wang, Y. Wan, K. Lin, et al., Gaseous sulfur trioxide induced controllable sulfonation promoting biomineralization and osseointegration of polyetheretherketone implants, Bioact. Mater. 5 (4) (2020) 1004–1017.
[37] X. Xu, Y. Li, L. Wang, Y. Li, J. Pan, X. Fu, et al., Triple-functional polyetheretherketone surface with enhanced bacteriostasis and anti-inflammatory and osseointegrative properties for implant application, Biomaterials 212 (2019) 98–114.
[38] X. Yuan, L. Ouyang, Y. Luo, Z. Sun, C. Yang, J. Wang, et al., Multifunctional sulfonated polyetheretherketone coating with beta-defensin-14 for yielding durable and broad-spectrum antibacterial activity and osseointegration, Acta Biomater. 86 (2019) 323–337.
[39] R. Ding, T. Chen, Q. Xu, R. Wei, B. Feng, J. Weng, et al., Mixed modification of the surface microstructure and chemical state of polyetheretherketone to improve its antimicrobial activity, hydrophilicity, cell adhesion, and bone integration, ACS Biomater. Sci. Eng. 6 (2) (2020) 842–851.
[40] L. Li, X. Shi, Z. Wang, Y. Wang, Z. Jiao, P. Zhang, In situ polymerization of poly (γ-benzyl-l-glutamate) on mesoporous hydroxyapatite with high graft amounts for the direct fabrication of biodegradable cell microcarriers and their osteogenic induction, J. Mater. Chem. B 6 (20) (2018) 3315–3330, https://doi.org/10.1039/c8tb00232k.
[41] W. Dong, W. Ma, S. Zhao, X. Zhou, Y. Wang, Z. Liu, D. Sun, M. Zhang, Z. Jiang, Multifunctional 3D sponge-like macroporous cryogel-modified long carbon fiber reinforced polyetheretherketone implants with enhanced vascularization and osseointegration, J. Mater. Chem. B 10 (28) (2022 Jul 20) 5473–5486, https://doi.org/10.1039/d2tb00725h. PMID: 35792102.
[42] Injectable mussel-inspired immobilization of platelet-rich plasma on microspheres bridging adipose micro-tissues to improve autologous fat transplantation by controlling release of PDGF and VEGF, angiogenesis, stem cell migration, Adv. Healthcare Mater. 6 (22) (2017 Nov), https://doi.org/10.1002/adhm.201700131. Epub 2017 Sep 7. PMID: 28881440.
[43] S. Chen, S. Cui, H. Zhang, et al., Cross-linked pectin nanofibers with enhanced cell adhesion, Biomacromolecules 19 (2) (2018) 490–498, https://doi.org/10.1021/acs.biomac.7b01605.
[44] J.R. Dondani, J. Iyer, S.D. Tran, Surface treatments of PEEK for osseointegration to, Bone. Biomol. 13 (3) (2023) 464, https://doi.org/10.3390/biom13030464. Published 2023 Mar 2.
[45] G. Jiang, S. Li, K. Yu, et al., A 3D-printed PRP-GelMA hydrogel promotes osteochondral regeneration through M2 macrophage polarization in a rabbit model, Acta Biomater. 128 (2021) 150–162, https://doi.org/10.1016/j.actbio.2021.04.010.
[46] J. Heinz Joist, G. Dolezel, J.V. Lloyd, R.L. Kinlough-Rathbone, J.F. Mustard, Platelet factor-3 availability and the platelet release reaction, J. Lab. Clin. Med. 84 (4) (1974) 474–482.
[47] S. Wei, P. Xu, Z. Yao, et al., A composite hydrogel with co-delivery of antimicrobial peptides and platelet-rich plasma to enhance healing of infected wounds in diabetes, Acta Biomater. 124 (2021) 205–218, https://doi.org/10.1016/j.actbio.2021.01.046.
[48] W. Pan, C. Dai, Y. Li, et al., PRP-chitosan thermoresponsive hydrogel combined with black phosphorus nanosheets as injectable biomaterial for biotherapy and phototherapy treatment of rheumatoid arthritis, Biomaterials 239 (2020), 119851, https://doi.org/10.1016/j.biomaterials.2020.119851.
[49] J. Grenier, H. Duval, F. Barou, P. Lv, B. David, D. Letourneur, Mechanisms of pore formation in hydrogel scaffolds textured by freeze-drying, Acta Biomater. 94 (2019) 195–203.
[50] H. Yoshida, T. Hatakeyama, H. Hatakeyama, Characterization of water in polysaccharide hydrogels by DSC, J. Therm. Anal. 40 (1993) 483–489.
[51] P. Jayabalan, T.J. Schnitzer, Tanezumab in the treatment of chronic musculoskeletal conditions, Expet Opin. Biol. Ther. 17 (2) (2017 Feb) 245–254, https://doi.org/10.1080/14712598.2017.1271873. Epub 2016 Dec 25.
[52] M.S. Bae, D.H. Yang, J.B. Lee, D.N. Heo, Y.D. Kwon, I.C. Youn, K. Choi, J.H. Hong, G.T. Kim, Y.S. Choi, E.H. Hwang, I.K. Kwon, Photo-cured hyaluronic acid-based hydrogels containing simvastatin as a bone tissue regeneration scaffold, Biomaterials 32 (32) (2011 Nov) 8161–8171.
[53] A. Fakhari, C. Berkland, Applications and emerging trends of hyaluronic acid in tissue engineering, as a dermal filler and in osteoarthritis treatment, Acta Biomater. 9 (7) (2013 Jul) 7081–7092.
[54] S.J. Falcone, D. Palmeri, R.A. Berg, et al., Biomedical applications of hyaluronic acid, Acs Symp. 934 (6) (2006) 155–174.
[55] E.R. Luvizuto, S. Tangl, T. Dobsak, et al., Effect of recombinant PDGF-BB on bone formation in the presence of β-tricalcium phosphate and bovine bone mineral matrix: a pilot study in rat calvarial defects, BMC Oral Health 16 (1) (2016) 52, 2016 May 4.
[56] J.C. Silva de Oliveira, R. Okamoto, C.K. Sonoda, W.R. Poi, I.R. Garcia Júnior, E. R. Luvizuto, Evaluation of the osteoinductive effect of PDGF-BB associated with different carriers in bone regeneration in bone surgical defects in rats, Implant Dent. 26 (4) (2017) 559–566.
[57] H.J. Kim, K.H. Kim, Y.M. Lee, Y. Ku, I.C. Rhyu, Y.J. Seol, ovariectomy-induced osteoporotic rat models, BMP-2 substantially reversed an impaired alveolar bone regeneration whereas PDGF-BB failed, Clin. Oral Invest. 25 (11) (2021) 6159–6170.
[58] A. Grosso, A. Lunger, M.G. Burger, et al., VEGF dose controls the coupling of angiogenesis and osteogenesis in engineered bone, NPJ Regen. Med. 8 (1) (2023) 15.
[59] R.J. Nagao, R. Marcu, Y. Wang, et al., Transforming endothelium with platelet-rich plasma in engineered microvessels, Adv. Sci. 6 (24) (2019), 1901725, 2019 Oct 16.
[60] M. Yada, K. Yamaguchi, T. Tsuji, NGF stimulates differentiation of osteoblastic MC3T3-E1 cells, Biochem. Biophys. Res. Commun. 205 (2) (1994 Dec 15) 1187–1193.
[61] M. Mogi, A. Kondo, K. Kinpara, A. Togari, Anti-apoptotic action of nerve growth factor in mouse osteoblastic cell line, Life Sci. 67 (10) (2000) 1197–1206.
[62] J. Xu, Z. Li, R.J. Tower, et al., NGF-p75 signaling coordinates skeletal cell migration during bone repair, Sci. Adv. 8 (11) (2022), eabl5716.